



Effect of a Ag nanoparticle filler on the performance and antibiofouling properties of a polyvinylidene difluoride membrane

Xingtao Zuo^a, Jiajie He^a, Cong Ma^{b,c,*}, Juan Xiong^d

^aCollege of Resources and Environment, Huazhong Agricultural University, Wuhan 430070, China

^bDepartment of Chemical and Biomolecular Engineering, University of Connecticut, 191 Auditorium Rd. Unit 3222, Storrs, CT 06269-3222, USA, emails: macong_0805@126.com, hit.macong@gmail.com (C. Ma)

^cState Key Laboratory of Separation Membranes and Membrane Processes, School of Environmental and Chemical Engineering, Tianjin Polytechnic University, Tianjin, 300387, China

^dCollege of Science, Huazhong Agricultural University, Wuhan 430070, China, email: xiong@mail.hzau.edu.cn

Received 18 October 2017; Accepted 18 March 2018

ABSTRACT

A novel polyvinylidene difluoride (PVDF) membrane containing Ag nanoparticles (nAg) was fabricated via a phase inversion method. The effect of the content of nAg on the performance of these membranes was extensively characterized. Antibacterial tests were also performed to examine the ability of the PVDF-Ag membranes to overcome biofouling. Scanning electron microscopy, Fourier transform infrared spectroscopy, and X-ray diffraction results confirmed the presence of nAg in the polymer matrix. The hydrophilic nature and antibacterial capacity of the membranes both depended on the nAg content of the membrane matrix (i.e., these parameters increased with the nAg content). On the other hand, the fouling mechanism of the prepared membranes was not modified upon incorporation of nAg. The PVDF membrane containing 0.2 wt% of nAg exhibited optimum transport properties, thereby showing great potential for developing high-performance antifouling membranes for separation processes.

Keywords: Ag nanoparticles; PVDF; Antifouling; Antibacterial; Fouling mechanism

1. Introduction

The rapid growth of nanotechnology has spurred significant interest in the fabrication of nanomaterials with environmental applications [1,2]. These materials are believed to have potential to revolutionize century-old conventional water treatment processes [3–5]. Several antimicrobial nanomaterials such as chitosan, Ag nanoparticles (nAg), TiO₂, and carbon nanotubes (CNTs) have shown potential to replace traditional chemical disinfectants prone to generate harmful disinfection byproducts [6]. The incorporation of nanomaterials into membrane-forming materials allows achieving multiple treatments in one single process while minimizing fouling [7,8].

nAg are one of the most extensively studied biocides, being effective against various aquatic microorganisms including bacteria, fungi, and algae, among others [9]. nAg blended in membrane fabrication process (i.e., phase inversion) to improve biofouling resistance and virus removal properties of nanocomposite microfiltration, ultrafiltration, nanofiltration, and reverse osmosis membranes [10–12]. nAg-filled polyimide, polyamide, chitosan, and polyethersulfone composite membranes have been synthesized. Among the organic polymer membrane materials, polyvinylidene difluoride (PVDF), having excellent physico-chemical properties, has attracted considerable attention for industrial applications. However, PVDF membranes suffer from fouling, which hinders their efficient applications. It is reported that silver ions were loaded on the (poly(acrylic acid) [PAA]) grafted layer on PVDF membrane surface by

* Corresponding author.

the coordination bond formed between carboxyl group of PAA and silver ion [13]. To the best of our knowledge, the performance of nAg-blended PVDF polymeric membranes has been scarcely studied.

In this work, nAg-embedded PVDF membranes were prepared with nAg as an additive via blending method A set of analyses including scanning electron microscopy (SEM), Fourier transform infrared spectroscopy (FTIR), X-ray diffraction (XRD), contact angle measurements, and membrane separation tests were carried out to characterize the membranes. Furthermore, classic fouling models were employed to investigate the effect of nAg on the fouling mechanism taking place on the PVDF membrane.

2. Materials and methods

2.1. Materials

PVDF (FR904, MW: 600,000) was obtained from 3F New Materials Co., Ltd., China. nAg ($\geq 99.9\%$) was 60–120 nm used as received (Aladdin Industrial Inc., China). Polyvinyl pyrrolidone (PVP, k30), dimethylacetamide (DMAC, $\geq 99.0\%$) and bovine serum albumin (BSA, $\geq 96.0\%$; National Chemical Reagent Co., Ltd., China) were used as obtained. All reagents were employed as received without further purification. Double-distilled water was used for the preparation of all the solutions.

2.2. Membrane preparation

Several PVDF/nAg composite membranes with varying nAg loadings (i.e., 0, 0.1, 0.2, 0.3, 0.4, and 0.5 wt% based on the total weight of the membrane-forming materials) were prepared. Viscous slurries were obtained by mixing PVDF, Ag, and PVP in DMAC at a fixed PVDF:PVP ratio of 7:0.1 (w/w). The resulting mixtures were left for 24 h to remove air bubbles. Gels were subsequently obtained and cast on clean glass plates using a doctor blade. The glass plates were subsequently immersed in a coagulation water bath. The as-formed membranes were washed and stored in ultrapure water before use. These membranes were designated as PVDF/Ag-X, where X is the nAg content (wt%) in the membrane phase.

2.3. Membrane characterization

2.3.1. Membrane morphology

The morphologies of these membranes were studied by SEM on a S4800HSD microscope (Japan). Both the membrane upper surfaces and cross-sections through the membrane were examined. The cross-sections of the membranes were prepared by fracturing them in liquid N_2 . All samples were sputtered with a thin conductive layer of Au/Pd prior to imaging.

2.3.2. FTIR-attenuated total reflection analyses

The FTIR-attenuated total reflection (ATR) spectra of the composite membranes were recorded on a FTIR spectrometer equipped with an ATR accessory (Equinox 55, Bruker, Japan) within 4,000–500 cm^{-1} .

2.3.3. XRD analyses

The XRD analyses of membranes were conducted with a diffractometer (D8 Advance, Bruker, German) equipped with monochromatic Cu- α radiation ($\lambda = 0.154$ nm) under a voltage of 40 kV and a current of 40 mA. All samples were analyzed in continuous scan mode with 2θ ranging from 10° to 80° .

2.3.4. Hydrophilicity, porosity, and pore size measurements

The hydrophilicity of the membranes was studied via water contact angle measurements. Contact angles were obtained on an optical tensiometer (ZSA25, Kruss, German) equipped with an image processing software. The contact angle values were average of at least five measurements.

The membrane porosity (ϵ) was determined via gravimetric analysis using Eq. (1):

$$\epsilon = \frac{(m_1 - m_2) / \rho_w}{(m_1 - m_2) / \rho_w + m_2 / \rho_m} \quad (1)$$

where m_1 and m_2 are the weights of the wet and dry membrane, respectively, while ρ_w and ρ_m are the densities of water and dry membrane, respectively.

The average pore size (d) of the membrane can be calculated from the pure water flux by the Guerout–Elford–Ferry equation [14]:

$$d = \sqrt{\frac{(2.9 - 1.75\epsilon) \times 8\mu l V_w}{\epsilon \times A \times \Delta P \times t}} \quad (2)$$

where μ is the water viscosity (8.9×10^{-4} Pa s), l is the membrane thickness, V_w is the volume of pure water penetrating through the membrane during an experimental time interval t . The effective membrane surface area (A) and the working pressure (ΔP) were 43.0×10^{-4} cm^2 and 0.1 MPa, respectively.

2.4. Membrane filtration tests

The separation performance of the membranes was investigated by conducting batch tests using a dead-end cell under constant pressure. A N_2 gas cylinder was used to pressurize the system to the desired operating pressure. Once the applied pressure was reached, the filtrate was collected and recorded continuously at equal time interval.

The flux (J_t) of the feed solution versus time was calculated as follows:

$$J_t = \frac{V}{A\Delta t} \quad (3)$$

where V is the permeate volume and Δt is the time. The corresponding filtration resistance (R_t) was determined according to the Darcy's law:

$$R_t = \frac{\Delta P}{\mu J_t} \quad (4)$$

where μ is the feed water viscosity.

The BSA rejection (R) was measured at a solute concentration of 1 g/L using a UV–Vis analyser according to Eq. (5):

$$R = \left(1 - \frac{C_p}{C_f} \right) \times 100\% \quad (5)$$

where C_p and C_f are the BSA concentration of the filtrate and feed solutions, respectively.

2.5. Membrane fouling index

The modified fouling index (MFI) developed by Boerlage et al. [15] and Arabi and Nakhla [16] was suggested for evaluating the fouling potential of feed water based on the cake filtration model and the Darcy's law [17]. MFI is defined as the slope of the linear portion of the t/V versus V filtration curve. It can be also represented as follows:

$$\frac{t}{V} = \frac{\mu R_m}{\Delta P A} + \left[\frac{\mu \alpha C_b}{2 \Delta P A^2} \right] V \quad (6)$$

where μ is the viscosity of the filtrate (Pa s), R_m is the membrane resistance, C_b is the concentration of macromolecules in the bulk solution (kg/m³), and α is the specific resistance (m/kg).

2.6. Modeling of the membrane fouling process

To better understand the fouling behavior of BSA, the flux decline of the membrane in the dead-end cell under constant pressure can be described by different blocking mechanisms [18] namely, complete blocking, standard blocking, intermediate blocking, and cake filtration. The equations describing the four classic fouling models are listed in Table 1 [19].

3. Results and discussion

3.1. Morphology

Fig. 1 shows the surface and cross-section SEM images of the membranes with different compositions. The surface images revealed a highly homogeneous pore structure in all cases, although nAg aggregation was observed for highly loaded membranes. There was no apparent difference among the cross sections of the fabricated membranes. A typical asymmetric and highly inhomogeneous structure was observed in all cases. This structure contained a dense

skin layer (i.e., selective top layer) linked by a considerably thicker finger-like porous sublayer.

3.2. FTIR and XRD studies

Fig. 2 shows the FTIR spectra of the prepared membranes. A strong absorbance was observed at 1,180 cm⁻¹ and ascribed to the stretching vibration of the CF bond. The bands observed at 1,402; 1,070; 875; 839; and 762 cm⁻¹ were produced by the stretching vibration of the CF₂ groups in the β -PVDF polymorphic phase [20,21]. The relative intensity of these bands increased upon incorporation of nAg (Fig. S1), suggesting that the addition of Ag enhanced the crystallization of the β -PVDF phase. No new bands were observed after addition of nAg to the PVDF matrix, thereby revealing a physical interaction between nAg and PVDF.

The XRD patterns of the pristine PVDF and PVDF/Ag membranes are shown in Fig. 3. The diffraction peaks obtained at 2 θ values of 18.5°, 20.2°, and 26.6° corresponded to the (020), (110), and (022) reflections of PVDF, while the signals at 38.1° and 44.2° were characteristics of nAg, in line with previous results [22,23].

The diffraction pattern of the nAg-embedded PVDF membranes showed peaks at 18.5°, 20.2°, 38.1°, and 44.4°, revealing that nAg were distributed within the PVDF membrane matrix. Moreover, the intensities of these diffraction peaks increased to different degrees with the nAg loading, thereby revealing enhanced crystallization, formation of large crystallites, and/or well-ordered orientation.

3.3. Membrane porosity and pore size

The porosity and pore size characteristics of the prepared membranes are shown in Fig. 4. The modified membranes showed lower porosity as compared with their pristine PVDF counterpart. The porosity of the modified membranes first decreased with the nAg loading (up to 0.3 wt%) and increased thereafter (0.3–0.5 wt%). These results are in line with those reported by Efome et al. [24]. These authors found the neat membrane to present higher porosity than the modified membranes, and this decrease was related to the increased viscosity produced by the addition of nanoparticles to the casting solution. The exchange rate of the solvent and non-solvent (water) increased with the concentration of nAg, thereby potentially resulting in membranes with higher porosity at nAg contents of 0.3–0.5 wt% in the casting solution.

The mean pore radius of the membranes increased with the nAg content up to 0.3 wt% (from 91.46 nm for the pristine PVDF to 184.00 nm for the PVDF/Ag-0.3) and decreased thereafter. The incorporation of nAg resulted in weaker solvent–polymer interactions, increasing the exchange rate between the solvent and non-solvent and forming macrovoids as a result. This was ascribed to a weakening effect of the nanoparticles as a result of agglomeration phenomena at high loadings, this leading to membrane pore clogging [25]. Thus, the presence of nanoparticles unevenly dispersed in the casting solution would result in membrane pore blockage and lower pore sizes as a result.

The viscosity of the casting solution was one of the major factors affecting the pore size of the membranes prepared by a phase inversion process. Thus, the addition of nAg increased

Table 1
Equations describing the different fouling mechanisms for dead-end filtration

Models	Equations
Complete blocking	$J_0 - J = aV$
Standard blocking	$1/t + b = J_0/V$
Intermediate blocking	$\ln J_0 - \ln J = cV$
Cake filtration	$(1/J) - (1/J_0) = dV$

Note: a , b , c , and d are constants.

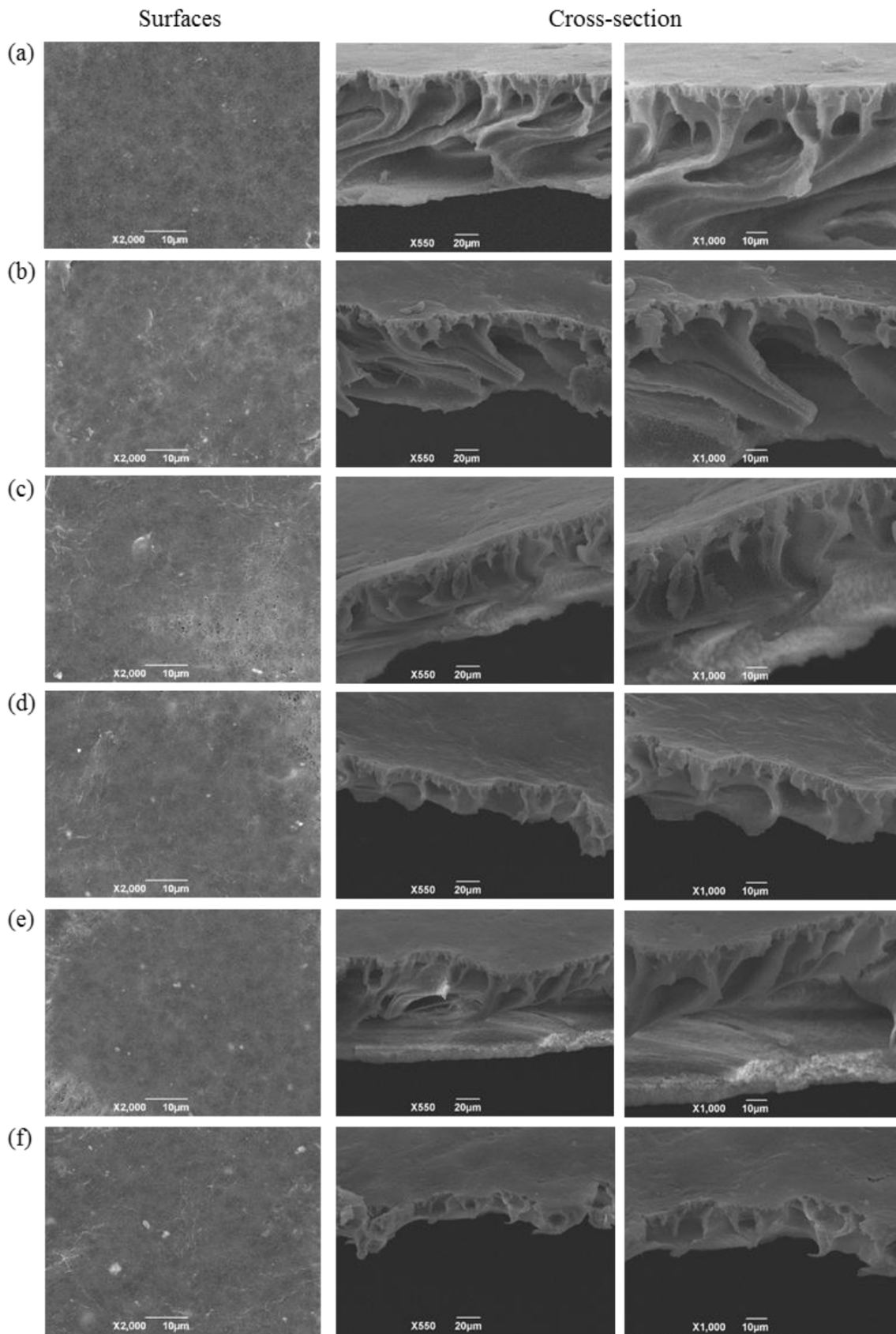


Fig. 1. SEM images of the surface and cross sections of the PVDF/Ag-X membranes: (a) $X = 0$; (b) $X = 0.1$; (c) $X = 0.2$; (d) $X = 0.3$; (e) $X = 0.4$; and (f) $X = 0.5$.

the viscosity of the casting solution, thereby hindering the mass transfer between the solvent and non-solvent phases [14]. Meanwhile, the formation of a nanoparticle network hindered the movement of the PVDF chains, avoiding the formation of macrovoid structures and decreasing the pore size [26].

3.4. Pure water flux and BSA rejection tests

The effect of nAg on the contact angles of the fabricated membranes containing different loadings of nanoparticles is shown in Fig. 5. The contact angle values decreased linearly with the nAg content of the membrane matrix. Thus, the addition of nAg resulted in PVDF membranes with higher surface hydrophilicity, in line with previous reports [22,23]. nAg were successfully dispersed and embedded within the hydrophobic PVDF membrane phase. The presence of nAg on the membrane surface facilitated the formation of a layer of water molecules, increasing the adsorption capacity

toward water and improving the hydrophilicity of the PVDF membrane as a result. As reported by Alhoshan et al. [25], the incorporation of a hydrophilic nanomaterial into a membrane matrix changed the membrane surface density and increased the surface energy, and thus water could easily spread on the surface.

The effect of the nAg content on the pure water flux and BSA rejection of the membranes is also depicted in Fig. 5. The higher hydrophilicity of the membranes produced a significant effect on the pure water flux. However, as shown in Fig. 5, a consistent tendency between flux and hydrophilicity was not found. The water flux decreased from 196.34 L/(m² h)

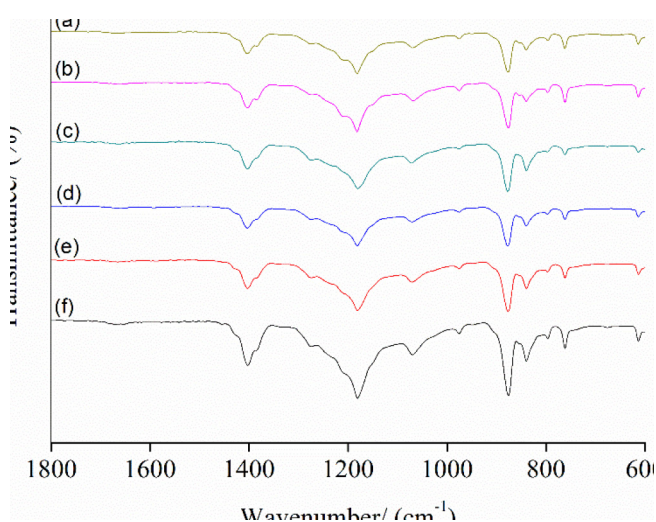


Fig. 2. FTIR spectra of the PVDF/Ag-X membranes: (a) $X = 0$; (b) $X = 0.1$; (c) $X = 0.2$; (d) $X = 0.3$; (e) $X = 0.4$; and (f) $X = 0.5$.

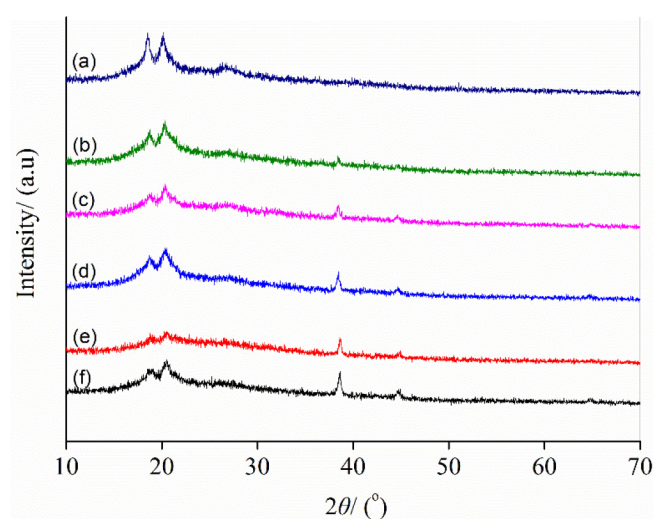


Fig. 3. XRD patterns of the PVDF/Ag-X membranes: (a) $X = 0$; (b) $X = 0.1$; (c) $X = 0.2$; (d) $X = 0.3$; (e) $X = 0.4$; and (f) $X = 0.5$.

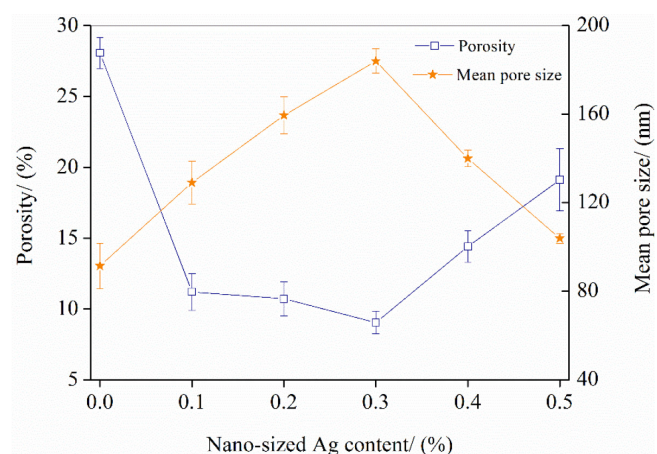


Fig. 4. Porosity and pore size of the prepared membranes.

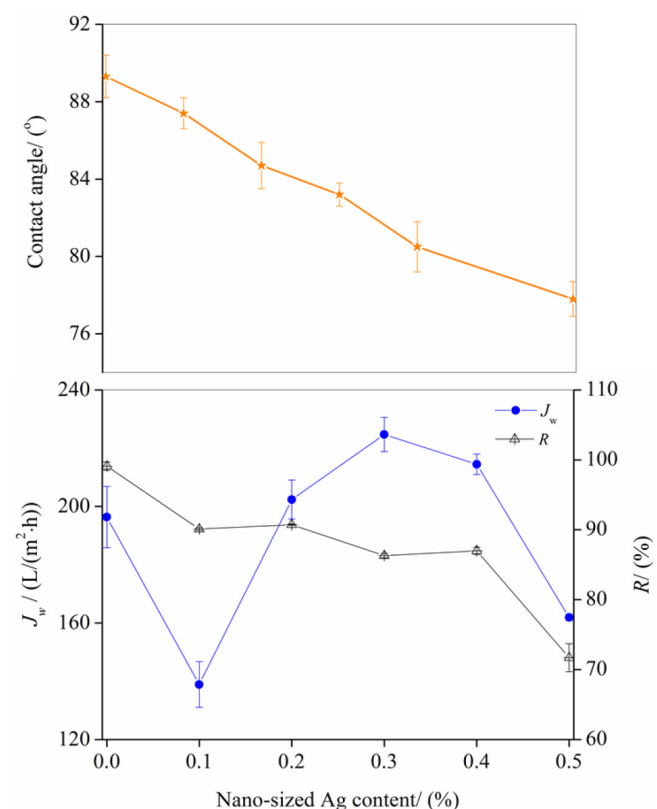


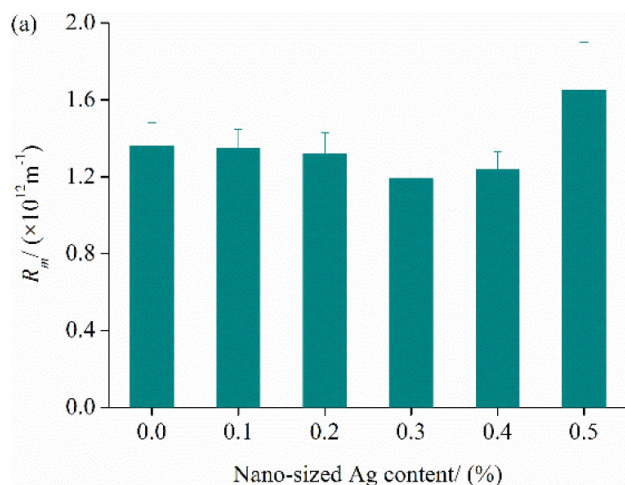
Fig. 5. Pure water fluxes and BSA rejection of the membranes.

for the pristine PVDF membrane to 138.88 L/(m² h) for the PVDF/Ag-0.1 membrane. The pure water flux increased with the nAg content (0.1–0.3 wt%) owing to the higher pore size and the enhanced hydrophilicity of the membranes. Despite showing improved hydrophilicity, the PVDF/Ag-0.5 membrane showed a lower flux as compared with the pristine PVDF membrane. The pure water flux changed following the same trend of the mean pore size. Thus, the pure water flux was influenced by the membrane pore size. It is inferred that the water flux decreased because of: (i) the decrease in the pore radius or (ii) the obstruction of the membrane pores, caused by the agglomeration of nanomaterial. The over addition of nanoparticles has been reported to result in permeability loss and changes in the membrane microstructure [27]. It can be concluded that not only hydrophilicity but also pore property was responsible for the water flux alteration, and moreover, pore property was the main contributor.

The rejection of all the fabricated membranes was investigated by employing BSA as a model organic foulant. The BSA rejection decreased with the nAg content, and the modified membranes showed lower rejection values than the pristine PVDF membrane. The rejection was lower than 90% for the membranes prepared with nAg contents higher than 0.2 wt%. The formation of macrovoids upon addition of nAg resulted in the lower BSA rejections [28]. These results suggested that the change of the pore size negatively affected the BSA rejection by the membranes, despite the enhanced hydrophilicity of the membranes could reduce the adsorption of organic pollutants within the membrane structure [29]. Therefore, the addition of optimum amounts of nAg to the membrane could improve the BSA rejection values. In this sense, 0.2 wt% was found to be proper nAg loading for modified PVDF nanocomposite membranes.

3.5. Membrane filtration resistance

The effect of the nAg content on the membrane resistance is shown in Fig. 6(a). The membrane resistance slightly decreased with the nAg content (up to 0.4 wt%), and increased sharply thereafter (0.5 wt%). PVDF/Ag-0.3 showed the lowest membrane resistance (12.5% lower than that of the neat PVDF) among the membranes under study.



The PVDF/Ag-0.5 membrane showed higher resistance than its pristine PVDF counterpart. The increased hydrophilicity of the membranes resulted in enhanced permeabilities and lower membrane resistances. The reasons for the PVDF/Ag membranes more easily fouled may be: (i) the pore sizes of all the PVDF/Ag membrane were larger than contaminants, which made it easy for the contaminants to adsorb and/or deposit onto the pore surface to make a pore blocking [30]. (ii) An increased surface porosity of the membrane made the pore blocking easier. The above behavior may be responsible for the observed trend of the membrane resistance.

The total resistance toward BSA filtration of the prepared membranes was also investigated as a function of time, and the results are illustrated in Fig. 6(b). Pristine PVDF showed significantly higher total resistance values than the modified membranes. PVDF/Ag-0.5 showed the largest filtration resistance of the Ag-modified PVDF membranes. PVDF/Ag-0.1 and PVDF/Ag-0.3 membranes exhibited relative lower total filtration resistance values. Especially, the PVDF/Ag-0.3 membrane showed the lowest R_t value for the filtration period (33.33% and 48.48% lower than that of the PVDF membrane for the initial and later periods, respectively). Unlike the pristine PVDF, the drop of the total filtration resistance for the modified membranes increased with the filtration time.

The total filtration resistance was noticeably higher (2–4 fold) than the membrane resistance, revealing that a significant amount of BSA was trapped by the membrane and subsequently deposited on the membrane surface and pore, resulting in membrane fouling and higher total filtration resistance. The highly hydrophilic structure induced by the nanomaterial was aimed to increase the affinity of these nanoparticles to water versus organic matter [31], resulting in lower hydraulic resistance of the nAg-embedded PVDF membranes. Optimum incorporation of nAg into the PVDF membrane phase not only reduced the membrane resistance but also the total resistance toward BSA filtration.

3.6. MFI

The t/V versus V filtration data were obtained for the constant pressure filtration of a BSA solution (1 g/L). The MFI values of the prepared membranes are shown in Fig. 7.

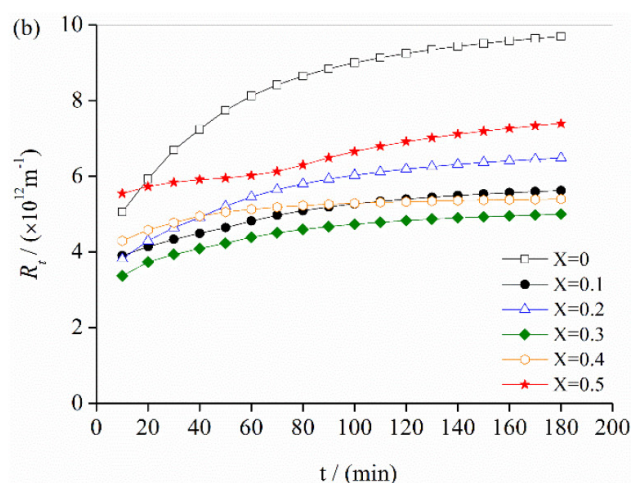


Fig. 6. Effect of nano-Ag content on filtration resistance: (a) membrane resistance and (b) total filtration resistance toward BSA.

The Ag-modified membranes showed significantly lower MFI values (by 86%–98%, values lower than 10^4 s/L²) than the pristine material. Moreover, the total resistance toward BSA filtration was significantly higher than the membrane resistance (from 10- to 36-fold). BSA was easily adsorbed on the surface of pristine PVDF, entering into the pores of the membrane, blocking them and producing

membrane fouling. In the presence of nAg, the improved hydrophilicity and permeability of the modified PVDF membranes reduced the BSA–membrane interaction, hindering the adsorption and deposition of BSA on the membrane surface [32], and reducing the formation rate for cake layers. Additionally, the higher MFI of the PVDF/Ag membranes may be attributed to the higher total filtration resistance and membrane resistance values of the modified membranes.

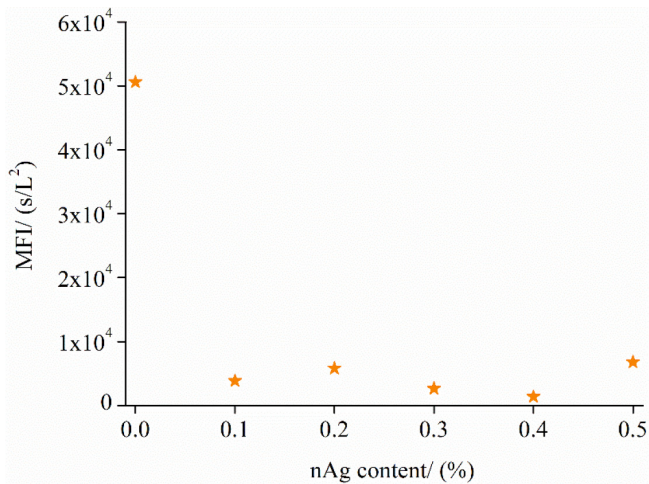


Fig. 7. Effect of the nAg content on the MFI of the prepared membranes.

3.7. Antibacterial performance

A gram-negative bacteria species such as *Escherichia coli* was selected as the biofoulant for analyzing the inhibition rate (dilution plate method) according to the number of viable colonies, and the results are shown in Fig. 8.

As shown in Fig. 8, the amount of bacterial colonies decreased with the nAg content of the membrane, suggesting that the antibacterial capacity of the PVDF/Ag membranes increased their nAg loading. As shown in Table 2, PVDF/Ag-0.5 showed the maximum antibacterial ratio, in good agreement with Kochkodan et al. [33] who reported a weakened adhesion of *E. coli* on hydrophilic membrane surfaces. According to Meng et al. [1] and Li et al. [6], this antibacterial mechanism can be explained in terms of Ag ions being released from the nanoparticles and disrupting the metabolism of the bacterial cells.

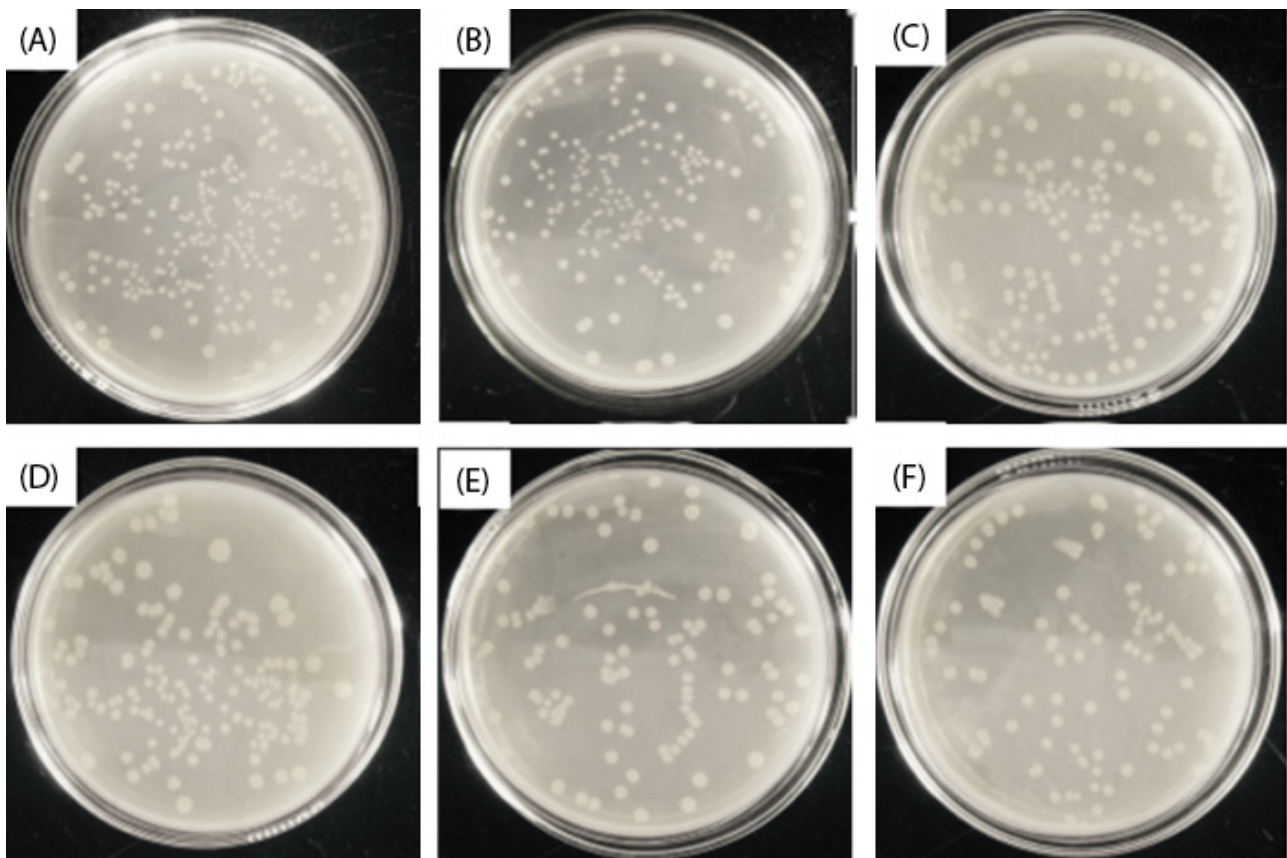


Fig. 8. Photographs showing the *E. coli* bacterial culture plates exposed to the membranes: (A) X = 0; (B) X = 0.1; (C) X = 0.2; (D) X = 0.3; (E) X = 0.4; and (F) X = 0.5.

Hence, these results highlighted the significant effect of the amount of incorporated nAg on the antibacterial property of the membranes. The enhanced antimicrobial properties of these membranes could be further applied to several separation and purification applications presenting biofouling issues.

3.8. Modeling of the filtration process of the BSA solution

Blocking models were applied to the constant pressure filtration of a BSA solution (1 g/L) with the aim to analyze the evolution of the BSA fouling on the prepared membranes. The permeate volume was measured as a function of time

Table 2
Antibacterial rate of the PVDF/Ag-X membranes

PVDF/Ag-X (%)	Antibacterial rate (%)
0.1	20.97
0.2	32.26
0.3	35.48
0.4	38.71
0.5	62.90

(3 h). The permeate volume versus time data was fit using four typical fouling models, and the results are shown in Fig. 9. The best fouling model was selected based on the best fitted equation (i.e., with the highest R^2 value in linear regression method) [34]. The resultant values of R^2 are summarized in Table 3.

The standard blocking model showed the best fit of the experimental data for the fabricated membranes ($R^2 > 0.98$). The cake filtration model provided a better fit as compared with the intermediate and complete blocking models. Thus, it is inferred that the main mechanism governing the flux decline by BSA was standard blocking. Herein, the formation of a cake did not show a significant effect on the membrane flux drop. This can be attributed to two factors: (i) the formation of a cake layer being restricted by the external cross flow caused by the high agitation, causing a sweeping effect on the membrane [35]; and (ii) a longer filtration time being required for the development of the cake layer. After addition of nAg to the PVDF membrane matrix, the standard blocking model fitted experimental data very well. This suggested that the incorporation of nAg and the loading of nanomaterial in the casting solution did not change the main membrane fouling mechanism of the prepared membranes during BSA filtration.

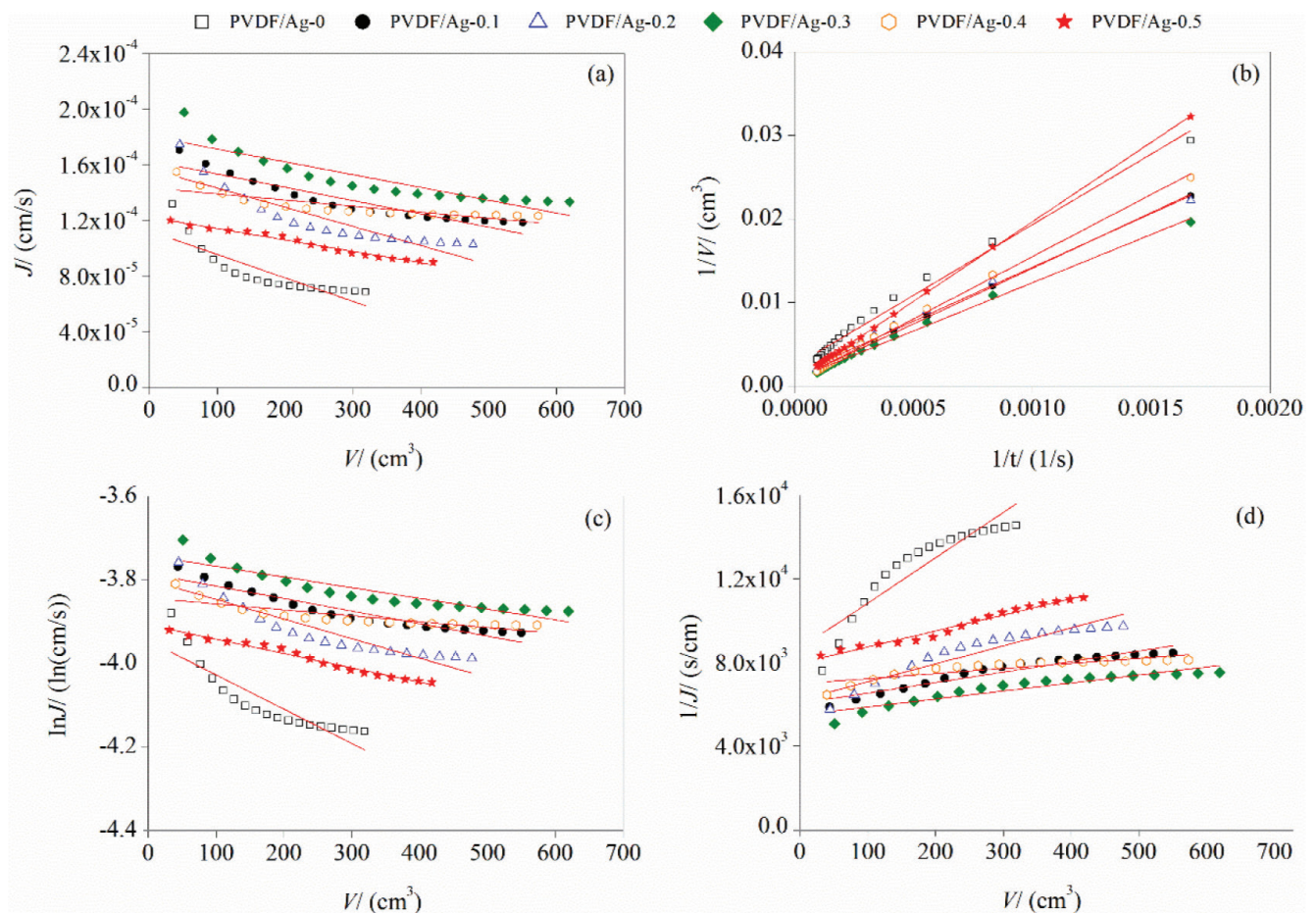


Fig. 9. Fitting of the flux decline of BSA by four models: (a) complete blocking; (b) standard blocking; (c) intermediate blocking; and (d) complete blocking.

Table 3
R² values of the four fitting models for the prepared membranes

Models	R ²					
	PVDF/Ag-X (%)					
	0	0.1	0.2	0.3	0.4	0.5
Complete blocking	0.711	0.876	0.790	0.797	0.683	0.980
Standard blocking	0.987	0.999	0.995	0.997	0.998	1.000
Intermediate blocking	0.783	0.903	0.841	0.837	0.709	0.979
Cake filtration	0.845	0.926	0.885	0.873	0.734	0.977

4. Conclusion

PVDF/Ag membranes were successfully fabricated with nAg. The hydrophilicity of the blended membranes was enhanced as compared with pristine PVDF. The porosity and improved hydrophilicity of the PVDF/Ag membranes decreased the membrane filtration resistance and MFI versus the PVDF membrane. The bactericidal capacity of the prepared membranes increased with the concentration of nAg in the membrane matrix, thereby reducing membrane biofouling. The PVDF/Ag-0.2 membrane showed optimum separation properties. The main fouling mechanism of the PVDF/Ag membranes during BSA filtration was standard blocking, regardless of the nAg concentration. The excellent antifouling performance and antimicrobial property of PVDF-Ag make them suitable material for membrane applications.

Acknowledgments

This work was supported by the Hubei Provincial Natural Science Foundation of China (No. 2016CFB495), the Fundamental Research Funds for the Central Universities of China (No. 2662017JC019), the National Science Foundation of China (No. 51508383) and the Research Fund of Tianjin Key Laboratory of Aquatic Science and Technology (No. TJKLAST-ZD-2017-03).

References

- [1] F. Meng, S. Zhang, Y. Oh, Z. Zhou, H.S. Shin, S.R. Chae, Fouling in membrane bioreactors: an updated review, *Water Res.*, 114 (2017) 151–180.
- [2] M.H. Habibi, M. Fakhrpor, Preparation of cerium zinc oxide nanocomposite derived by hydrothermal route coated on glass and its application in water treatment, *Desal. Wat. Treat.*, 57 (2016) 26204–26210.
- [3] M.A. Shannon, P.W. Bohn, M. Elimelech, J.G. Georgiadis, B.J. Marías, A.M. Mayes, Science and technology for water purification in the coming decades, *Nature*, 452 (2008) 301–310.
- [4] C. Santhosh, V. Velmurugan, G. Jacob, S.K. Jeong, A.N. Grace, A. Bhatnagar, Role of nanomaterials in water treatment applications: a review, *Chem. Eng. J.*, 306 (2016) 1116–1137.
- [5] S. Parastar, S. Nasser, S.H. Borji, M. Fazlzadeh, A.H. Mahvi, A.H. Javadi, M. Gholami, Application of Ag-doped TiO₂ nanoparticle prepared by photodeposition method for nitrate photocatalytic removal from aqueous solutions, *Desal. Wat. Treat.*, 51 (2013) 7137–7144.
- [6] Q. Li, S. Mahendra, D.Y. Lyon, L. Brunet, M.V. Liga, D. Li, P.J.J. Alvarez, Antimicrobial nanomaterials for water disinfection and microbial control: potential applications and implications, *Water Res.*, 42 (2008) 4591–4602.
- [7] X. Qu, P.J.J. Alvarez, Q. Li, Applications of nanotechnology in water and wastewater treatment, *Water Res.*, 47 (2013) 3931–3946.
- [8] K.J. Lee, E. Cha, H.D. Park, High antibiofouling property of vertically aligned carbon nanotube membranes at a low cross-flow velocity operation in different bacterial solutions, *Desal. Wat. Treat.*, 57 (2016) 23505–23515.
- [9] X. Liu, S. Qi, Y. Li, L. Yang, B. Cao, C.Y. Tang, Synthesis and characterization of novel antibacterial silver nanocomposite nanofiltration and forward osmosis membranes based on layer-by-layer assembly, *Water Res.*, 47 (2013) 3081–3092.
- [10] M. Ben-Sasson, X. Lu, E. Bar-Zeev, K.R. Zodrow, S. Nejati, G. Qi, E.P. Giannelis, M. Elimelech, In situ formation of silver nanoparticles on thin-film composite reverse osmosis membranes for biofouling mitigation, *Water Res.*, 62 (2014) 260–270.
- [11] K. Zodrow, L. Brunet, S. Mahendra, D. Li, A. Zhang, Q. Li, P.J.J. Alvarez, Polysulfone ultrafiltration membranes impregnated with silver nanoparticles show improved biofouling resistance and virus removal, *Water Res.*, 43 (2009) 715–723.
- [12] X. Hong, Y. Zhou, Z. Ye, H. Zhuang, W. Liu, K.S. Hui, Z. Zeng, X. Qiu, Enhanced hydrophilicity and antibacterial activity of PVDF ultrafiltration membrane using Ag₃PO₄/TiO₂ nanocomposite against *E. coli*, *Desal. Wat. Treat.*, 75 (2017) 26–33.
- [13] J.H. Li, X.S. Shao, Q. Zhou, M.Z. Li, Q.Q. Zhang, The double effects of silver nanoparticles on the PVDF membrane: surface hydrophilicity and antifouling performance, *Appl. Surf. Sci.*, 265 (2013) 663–670.
- [14] V. Vatanpour, S.S. Madaeni, A.R. Khataee, E. Salehi, S. Zinadini, H.A. Monfared, TiO₂ embedded mixed matrix PES nanocomposite membranes: influence of different sizes and types of nanoparticles on antifouling and performance, *Desalination*, 292 (2012) 19–29.
- [15] S.F.E. Boerlage, M.D. Kennedy, P.A.C. Bonne, G. Galjaard, J.C. Schippers, Prediction of flux decline in membrane systems due to particulate fouling, *Desalination*, 113 (1997) 231–233.
- [16] S. Arabi, G. Nakhla, Impact of molecular weight distribution of soluble microbial products on fouling in membrane bioreactors, *Sep. Purif. Technol.*, 73 (2010) 391–396.
- [17] Y. Jin, Y. Ju, H. Lee, S. Hong, Fouling potential evaluation by cake fouling index: theoretical development, measurements, and its implications for fouling mechanisms, *J. Membr. Sci.*, 490 (2015) 57–64.
- [18] J. Hermia, Constant pressure blocking filtration laws-application to power-law non-Newtonian fluids, *Trans. Inst. Chem. Eng.*, 60 (1982) 183–187.
- [19] W.R. Bowen, J.I. Calvo, A. Hernández, Steps of membrane blocking in flux decline during protein microfiltration, *J. Membr. Sci.*, 101 (1995) 153–165.
- [20] H.H. Tseng, G.L. Zhuang, Y.C. Su, The effect of blending ratio on the compatibility, morphology, thermal behavior and pure water permeation of asymmetric CAP/PVDF membranes, *Desalination*, 284 (2012) 269–278.
- [21] A.B. Radwan, A.M.A. Mohamed, A.M. Abdullah, M.A. Al-Maadeed, Corrosion protection of electrospun PVDF-ZnO superhydrophobic coating, *Surf. Coat. Technol.*, 289 (2016) 136–143.
- [22] V. Vatanpour, A. Shockravi, H. Zarrabi, Z. Nikjavan, A. Javadi, Fabrication and characterization of anti-fouling and antibacterial Ag-loaded graphene oxide/polyethersulfone mixed matrix membrane, *J. Ind. Eng. Chem.*, 30 (2015) 342–352.

- [23] J. Li, X. Liu, J. Lu, Y. Wang, G. Li, F. Zhao, Anti-bacterial properties of ultrafiltration membrane modified by graphene oxide with nano-silver particles, *J. Colloid Interface Sci.*, 484 (2016) 107–115.
- [24] J.E. Efome, M. Baghbanzadeh, D. Rana, T. Matsuura, C.Q. Lan, Effects of superhydrophobic SiO₂ nanoparticles on the performance of PVDF flat sheet membranes for vacuum membrane distillation, *Desalination*, 373 (2015) 47–57.
- [25] M. Alhoshan, J. Alam, L.A. Dass, N. Al-Homaidi, Fabrication of polysulfone/ZnO membrane: influence of ZnO nanoparticles on membrane characteristics, *Adv. Polym. Technol.*, 32 (2013) 21369.
- [26] L.Y. Yu, Z.L. Xu, H.M. Shen, H. Yang, Preparation and characterization of PVDF-SiO₂ composite hollow fiber UF membrane by sol-gel method, *J. Membr. Sci.*, 337 (2009) 257–265.
- [27] S. Liang, K. Xiao, Y. Mo, X. Huang, A novel ZnO nanoparticle blended polyvinylidene fluoride membrane for anti-irreversible fouling, *J. Membr. Sci.*, 394–395 (2012) 184–192.
- [28] X. Li, R. Pang, J. Li, X. Sun, J. Shen, W. Han, L. Wang, In situ formation of Ag nanoparticles in PVDF ultrafiltration membrane to mitigate organic and bacterial fouling, *Desalination*, 324 (2013) 48–56.
- [29] S. Balta, A. Sotto, P. Luis, L. Benea, B. Van der Bruggen, J. Kim, A new outlook on membrane enhancement with nanoparticles: the alternative of ZnO, *J. Membr. Sci.*, 389 (2012) 155–161.
- [30] X. Fu, T. Maruyama, T. Sotani, H. Matsuyama, Effect of surface morphology on membrane fouling by humic acid with the use of cellulose acetate butyrate hollow fiber membranes, *J. Membr. Sci.*, 320 (2008) 483–491.
- [31] Y.T. Chung, M.M. Ba-Abbad, A.W. Mohammad, A. Benamor, Functionalization of zinc oxide (ZnO) nanoparticles and its effects on polysulfone-ZnO membranes, *Desal. Wat. Treat.*, 57 (2016) 7801–7811.
- [32] E. Yuliwati, A.F. Ismail, Effect of additives concentration on the surface properties and performance of PVDF ultrafiltration membranes for refinery produced wastewater treatment, *Desalination*, 273 (2011) 226–234.
- [33] V.M. Kochkodan, N. Hilal, V.V. Goncharuk, L. Al-Khatib, T.I. Levadna, Effect of the surface modification of polymer membranes on their microbiological fouling, *Colloid J.*, 68 (2006) 267–273.
- [34] Y. Shen, W. Zhao, K. Xiao, X. Huang, A systematic insight into fouling propensity of soluble microbial products in membrane bioreactors based on hydrophobic interaction and size exclusion, *J. Membr. Sci.*, 346 (2010) 187–193.
- [35] I. Rosas, S. Collado, A. Gutiérrez, M. Díaz, Fouling mechanisms of *Pseudomonas putida* on PES microfiltration membranes, *J. Membr. Sci.*, 465 (2014) 27–33.

Supplementary material

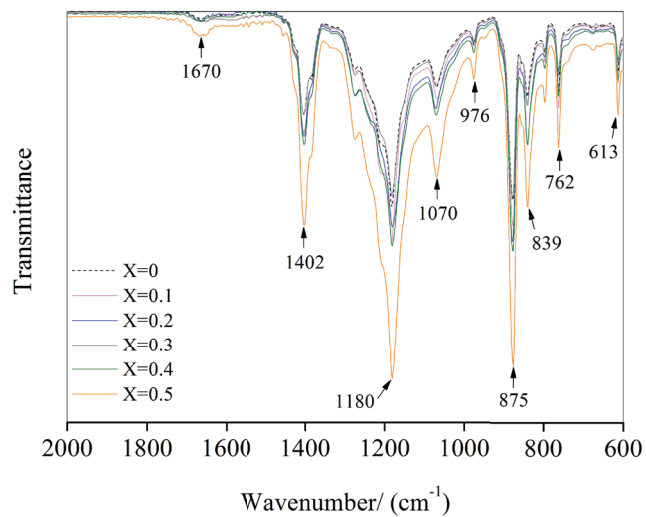


Fig. S1. FTIR spectra for the PVDF/Ag-X membranes.